Robotica: (2021) volume 39, pp. 1417–1433. © Tongji University, 2021. Published by Cambridge University Press.
doi:10.1017/S0263574720001253

Design and Implementation of a Cable Inspection Robot for Cable-Stayed Bridges

Zhipeng Wang†,‡, Bin He†,‡*, Yanmin Zhou†,‡, Ke Liu†,‡ and Chenghong Zhang†,‡

†*Department of Control Science and Engineering, Tongji University, No.4800 Caoan Road, Shanghai 201804, China*
‡*Shanghai Research Institute for Intelligent Autonomous Systems, No.55 Chuanhe Road, Shanghai 200120, China*
E-mails: wangzhipeng@tongji.edu.cn, yanmin.zhou@tongji.edu.cn, 1414358333@qq.com, 771996588@qq.com

(Accepted December 2, 2020. First published online: January 8, 2021)

SUMMARY
Cable is the most important bearing structure of the cable-stayed bridges. Its safety has been of crucial public concern. Traditional manual cable inspection method has many defects such as low inspection efficiency, poor reliability and hazardous working environment. In this paper, a new wirelessly controlled cable-climbing robot enabling safe and convenient inspection of stay cables is proposed. The designed robot is composed of two modules, joined by four turnbuckles to form a closed structure that clasps the cable. The robot is controlled wirelessly by a ground-based station, and a DC power is supplied via an onboard lithium battery. The climbing principle and mechanical structure of this robot are introduced. The static model of the robot during obstacle negotiation is established. The relationships of the driving force and resistance with obstacle height to determine the obstacle-negotiation capability of the robot are obtained. The effects of cable diameter, cable inclination and preload force on obstacle climbing ability of the robot are also analyzed. The experiments verify that the robot could climb random inclined cables and overcome an obstacle of 2.42 mm in height with a mass of 5 kg payload.

KEYWORDS: Climbing robot; Cable inspection; Climbing ability; Obstacle negotiation; Cable-stayed bridge.

1. Introduction

The healthy status of cable-stayed bridge is crucially important for personnel safety and social stability. The breakage of one or several components of the bridge may result in catastrophic accidents.[1]

As the most important stress components of cable-stayed bridges, cables are exposed to air, wind, rain, snow and sunshine for long durations. Along with their service time increase, cracks and pitting corrosion appear on the polyethylene (PE) sheathing layer of cables. Moreover, these cracks and corrosion of PE layer continue to occur and have led to serious problems such as the breakage of steel wires in the interior of cables.[2] Therefore, periodic inspection and maintenance of cables are critical to the safety of the bridge structure.

The traditional cable inspection method is visual inspection by trained workers, which is an inefficient and dangerous method. The inspection task is conducted by using winding engine and hanging

* Corresponding author. E-mail: hebin@tongji.edu.cn

basket held by steel ropes. However, this manual inspection method does not guarantee the safety of the worker. The weight of hanging basket with workers and equipment is about hundreds of kilograms, which may cause damages to the PE sheathing layer of cables. In addition, the long towing wire can easily get wrapped around the cable, making the inspection task impossible. Therefore, automated cable inspection mechanism is highly desirable. A robot can climb up the cable and monitor the status of the cable in place of workers through inspection sensors such as cameras and nondestructive test (NDT) devices. This automatic inspection method can ensure the safety of inspector and improve the task efficiency greatly.

The locomotion mode of climbing robot includes wheel type, crawler belt type, legged type and worming type. The robot-based wheel or crawler belt has the advantages of high locomotion speed, good load capacity and suitable for long distance locomotion task.[3] The legged robots such as quadruped or hexapod robots have exceptional environmental adaptability, which can walk through rough terrain.[4,5] The worming climbing robots can climb up complicated structures such as cables with branches.[6]

Recently, some climbing robots for pole-like structures have been developed for building maintenance. Guan et al.[7,8] designed a worming climbing robot Climbot. This robot not only has superior mobility on multiple climbing media, such as poles and trusses, but also has the function of grasping and manipulating objects. Lam et al.[9,10] proposed a bionic tree climbing robot Treebot that is capable of climbing from a tree trunk to a branch. Mahdavi et al.[11] proposed a UT-pole climbing robot (UT-PCR) to clean highway lighting poles, which is composed of a triangular body and six limbs with ordinary wheels at the tips. Tavakoli et al.[12] proposed a four-degree-of-freedom (DoF) climbing robot named PCR, which can travel along tubular structures with bends, branches and step changes in cross section. Mazumdar et al.[13] developed a legged robot with permanent magnets imbedded in each foot for steel bridge inspection. ATIS cable robot, a wheel-based cable-climbing robot developed by Alpin Technik Leipzig, was designed to meet various purposes of cable inspection and maintenance,[14] including visual inspection and magnetic flux leakage modules for inspection, coating modular and welding modules for maintenance. Lee et al.[15] proposed a wheel-based cable robot to as an exciter for evaluating damping ratios of a stay cable. Ho et al.[16] developed a damage detection algorithm for cable inspection based on this robot. Cho et al.[17–19] proposed climbing robots enabling inspection of the hanger cable. These robots can be wirelessly controlled by inspector on the ground, though AC power is supplied via a tether cable.[18] This limits the work height for large-span cable-stayed bridge inspection. Generally, complicated movements are not required due to the cables have no branches and bends. However, the cable-stayed bridges consist of hundreds of cables, which requires high inspection efficiency and reliability in high altitude. Therefore, the inspection robot usually uses minimum DoFs and drivers to enable efficient completion of inspection tasks.[18] Due to the advantage of simple structure, most of the cable or pole inspection robots employed the wheel-driven mode.[17–20]

Although there are various cable inspection robots in previous research, challenges remain to improve the performance of the inspection robot, such as heavy self-weight, complicated installation process and high-energy consumption. In this paper, we present a new climbing robot for cable inspection of cable-stayed bridges. The robot consists of two modules, joined by four turnbuckles to form a frame around the cable. It can be controlled wirelessly, and a DC power is supplied via an onboard lithium-polymer battery. The robot is 12 kg in weight and can carry a payload over 5 kg (the maximum design payload is 8 kg). The robot is able to inspect cable status with detect sensors in real time, while climbing up or down.

The remaining sections of this paper are organized as follows. The mechanisms of the robot are described in Section 2. The overall control system of the robot is introduced in Section 3. The obstacle-negotiation capability of the robot is analyzed in Section 4. The experiments of the developed robot and the results are then discussed in Section 5. Finally, conclusions are given in Section 6.

2. Mechanism Design for Cable-Climbing Robot

The cable-climbing robot is a wireless mobile platform with inspection and maintenance equipment. The robot should be able to have enough climbing ability to overcome the weight of the body and the resistance of obstacles. The structure of the stayed cable of cable-stayed bridge is shown in Fig. 1(a), which consists of two anchor cup, two anchor band, two connecting cylinder and one cable. The

https://doi.org/10.1017/S0263574720001253 Published online by Cambridge University Press

Table I. Specifications of the robot.

Parameter	**Value**
Dimensions	$(480-590)\times 260\times 300$ mm^3
Mass	12 kg
Applicable payload	>5 kg
Climbing angles	0–90°
Applicable cable diameters	90–200 mm
Climbing speed	0–9 m/min

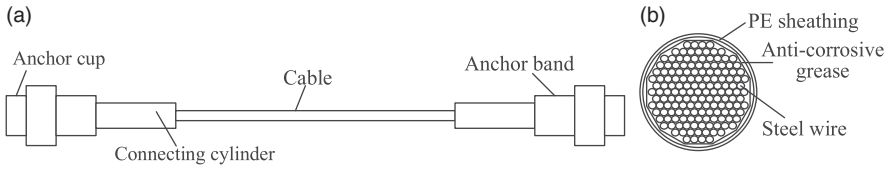

Fig. 1. The cable of the cable-stayed bridge. (a) The structure of the cable. (b) The cross section of the cable.

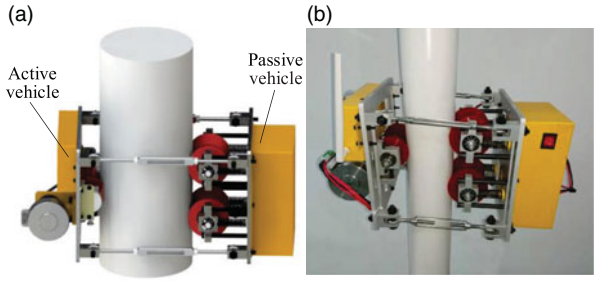

Fig. 2. Cable-climbing robot. (a) Three-dimension model. (b) Photograph.

cross section of the cable is shown in Fig. 1(b). The steel wire bundle is covered by a PE sheathing layer to reduce corrosion. However, there have been corrosion cracks and ridges distributed on the surface of the PE sheathing. This means that the cable-climbing robot should have good obstacle-negotiation capability. The weight of the robot can be considered as the load of the cable, and too heavy of which may cause damage to the PE sheathing. In addition, the cable inspection robot is a typical high altitude working device, to whose safety landing method should be considered.

The cable inspection robot is shown in Fig. 2. The detailed specifications of the robot are listed in Table I. In order to satisfy the requirements for cable inspection, the robot has the characteristics as follows:

1. To guarantee the sample structure and lightweight of the robot, the mechanism is driven by a brushless direct current (BLDC) motor. This improves the energy efficiency and avoids the out of step caused by multi-motor driving.
2. The driving unit should produce sufficient driving force, which makes the robot has good obstacle performance.
3. The robot should have high operation efficiency. It is easy to be installed by two workers and can efficiently navigate through cables that are several hundred meters long.
4. To satisfy safe landing demands, a one-way rotating damper is used to limit the fall down speed of the robot. To conserve energy, the BLDC motor can be used as generator to recharge the battery when the robot is climbing down.

The robot is composed of two vehicles, which are active vehicle and passive vehicle, as shown in Fig. 3. The two vehicles are connected by four turnbuckles to form a complete, closed frame that clasps the cable. The active vehicle is composed of a based board, a BLDC motor, a transmission mechanism, an active wheel, a one-way rotating damper and a belt-tensioning device. The passive

https://doi.org/10.1017/S0263574720001253 Published online by Cambridge University Press

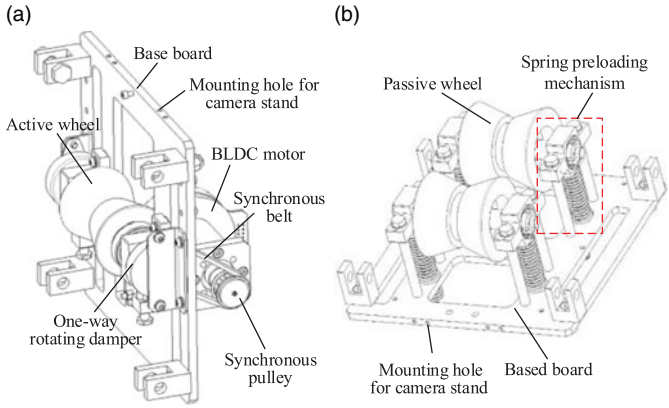

Fig. 3. The active vehicle and passive vehicle of the climbing robot. (a) Active vehicle. (b) Passive vehicle.

vehicle is composed of a based board, four spring preload mechanisms and two passive wheels. The spring preloading device generates the preload force (normal force) between the robot and the surface of the cable, which is important for the static friction of the active wheel. The compressed length of spring can be adjusted by rotating the turnbuckle. The tire of the wheels is made of rubber to improve the friction coefficient between the wheel and cable. In order to increase the contact area, the tire has a V groove. In addition, the four mounting holes on the based board of the active vehicle and passive vehicle are used for the fixing camera stand. Thus, the robot can be deployed with cameras to realize 360° view detection.

2.1. Driving mechanism

The requirements of driving mechanism are as follows:

1. The driving mechanism should have good payload capacity to carry cameras, NDT or other devices.
2. The motor should have lightweight, large output torque, low energy consumption and high precision.
3. The driving mechanism should be small and have simple structure to ensure the high working reliability of the robot.

Based on the above requirements, the driving mechanism is consisted of a BLDC motor, a planetary gear train, a pair of synchronous pulleys, a synchronous belt, a one-way rotating damper and an active wheel. In normal operation, the motor torque is transmitted to the wheel via the planetary gearbox and synchronous belt. However, in the case of electrical malfunction or power failure, the active wheel will rotate freely and the robot will slip down the cable from several hundred meters. In order to satisfy the demand of safe retrieval of the robot, the one-way rotating damper is introduced to control the landing speed, as shown in Fig. 4. When the robot climbs up the cable, the damper is loosened. While the robot slips down, the driving wheel drives the one-way damper. In the case of the robot gets stuck on the cable, it can be pulled back to the ground by a rescue climbing robot with electromagnetic or mechanical adsorption device.

The power of conventional cable inspection robot is supplied via tether cable. The long power wire will be a heavy load when the robot working in high altitude. It can be easily wrapped around the cable, causing malfunctions of the robot. In order to avoid the disadvantages of the tether cable for power supplying, the lithium-polymer battery is used as a power supply unit for the robot. The capacity of the battery is 10 Ah. The over current protection and battery indicator are configured in the power supply unit. In addition, the BLDC motor can be used as a generator to recharge the battery when the robot is climbing down without power.

In order to analyze the driving condition, the robot is simplified, as shown in Fig. 5. The driving force of the robot comes from the static friction of the active wheel. Therefore, the climbing success of the robot depends on not only the driving torque of motor but also the static friction coefficient

https://doi.org/10.1017/S0263574720001253 Published online by Cambridge University Press

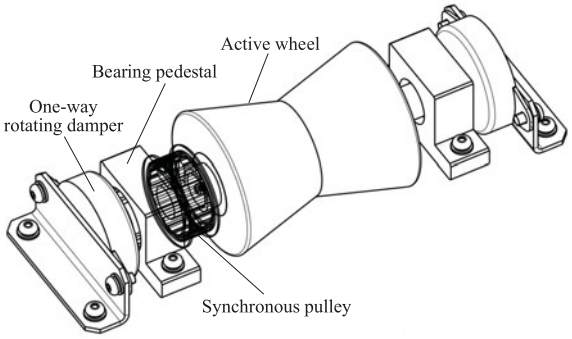

Fig. 4. Driving shaft.

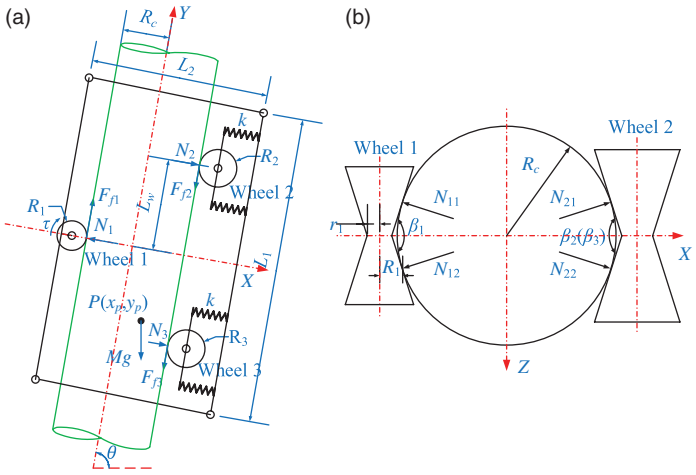

Fig. 5. Driving condition analysis. (a) Force diagram in XY plane. (b) Analysis of wheel contact force in XZ plane.

between the active wheel and cable surface. The maximum static friction force is directly proportional to the normal force applied to the active wheel by cable surface. The nonskid condition of the active wheel is written by:

$$F_{f1} = \mu_1 N_1 \geq \left(F_{f2} + F_{f3} + Mg \sin\theta\right) \sin\frac{\beta_1}{2}, \tag{1}$$

where μ_1 is the static friction coefficient, M is the mass of the robot, g is the gravitational acceleration, θ is the tilt angle of the cable, F_{f1} is the friction driving force of the active wheel, F_{f2} and F_{f3} are friction resistances of the upper and lower passive wheels, respectively, β_1 is the angle of V groove of the active wheel and N_1 is the equivalent normal force applied to the active wheel by the cable surface, which can be given by:

$$N_1 = N_{11} \sin\frac{\beta_1}{2} + N_{12} \sin\frac{\beta_1}{2} = 2N_{11} \sin\frac{\beta_1}{2}, \tag{2}$$

where N_{11} and N_{12} are the supporting forces by which the cable acts on two planes of the active wheel, N_{11}=N_{12}. The equivalent normal force applied to passive wheels can be obtained by the same way.

The driving condition of the active wheel is given by:

$$\tau_{\max} \geq \left(F_{f2} + F_{f3} + Mg \sin\theta\right) R_1, \tag{3}$$

https://doi.org/10.1017/S0263574720001253 Published online by Cambridge University Press

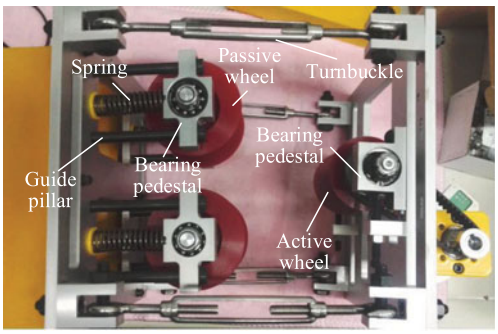

Fig. 6. Installation mechanism.

where τ_{max} is the maximum driving torque of the motor, and R_1 is the equivalent radius of active wheel, as shown in Fig. 4(b), which is as follows:

$$R_1 = r_1 + R_c \cos^2 \frac{\beta_1}{2} \Big/ \sin \frac{\beta_1}{2}, \tag{4}$$

where r_1 is the minimum radius of active wheel, as shown in Fig. 4(b), and R_c is the radius of the cable. The equivalent radius of passive wheels can be calculated by the same way.

Thus, we can select the proper driving motor and preload force based on Eqs. (1) and (3).

2.2. *Robot installation process*

The cables usually have varies diameters for different bridges. The preload mechanism of the robot needs to meet the requirement of cables with different diameters. In order to improve the working efficiency, a conveniently preload mechanism and installation method are very necessary for reducing the inspection time and cost. The preload force (normal force) is a critical factor influencing the climbing ability and safety of the inspection robot. Most of the existing cable inspection robots cannot measure the preload force during the installation procedure. Furthermore, some robot cannot adjust the preload force continuously. In order to install the robot conveniently, four-preload mechanism is designed. Each mechanism is composed of one spring, one bearing pedestal and two guide pillar for passive wheel, as shown in Fig. 6. The active vehicle and passive vehicle are connected by four turnbuckles. The turnbuckle is consisted of two threaded eye bolts, one screwed into each end of a small metal frame, one with a left-hand thread and the other with a right-hand thread. The preload force of the robot can be adjusted by rotating the frame, which causes both eye bolts to be screwed in or out simultaneously. The installation operation is as follows:

1. In order to install the robot on a hanger cable, the active vehicle is placed on the hanger cable in the first. Then, four turnbuckles are mounted on the active vehicle, as shown in Fig. 7(a).
2. The turnbuckles are adjusted to the maximum length, respectively. Then, the passive vehicle is placed on the other side of the cable, as shown in Fig. 7(b).
3. The turnbuckles are tightened until the passive wheels are just in contact with the cable surface, as shown in Fig. 7(c).
4. In order to ensure enough preload force and get the best climbing performance, the turnbuckle is adjusted to the optimal length, which is obtained by force analysis of the robot. The compressed length of each spring can be measured by the scale on the guide pillar, as shown in Fig. 7(d). This means that the preload force applied by the spring can be measured by the guide pillar during the procedure of robot installation.

The preload mechanism and installation method have good adaptability for varies cable diameters. The range of cable diameter can be expanded through changing turnbuckles of different sizes. The preload force can be calculated by the scale on the guide pillar. This ensures the preload mechanism can apply accuracy preload force for the lightweight climbing robot in the case of cable vibration. The entire procedure can be completed by two workers within 2 min.

https://doi.org/10.1017/S0263574720001253 Published online by Cambridge University Press

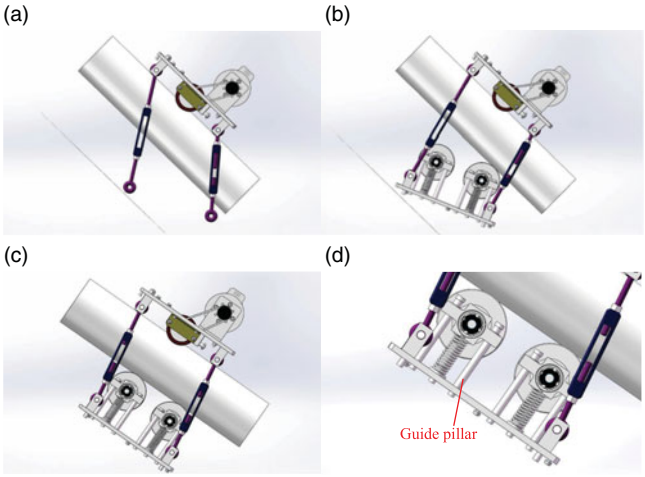

Fig. 7. Installation procedures of the cable inspection robot. (a) Installation of the active vehicle. (b) Installation of the passive vehicle. (c) Tightening the turnbuckles. (d) Adjusting the preload force.

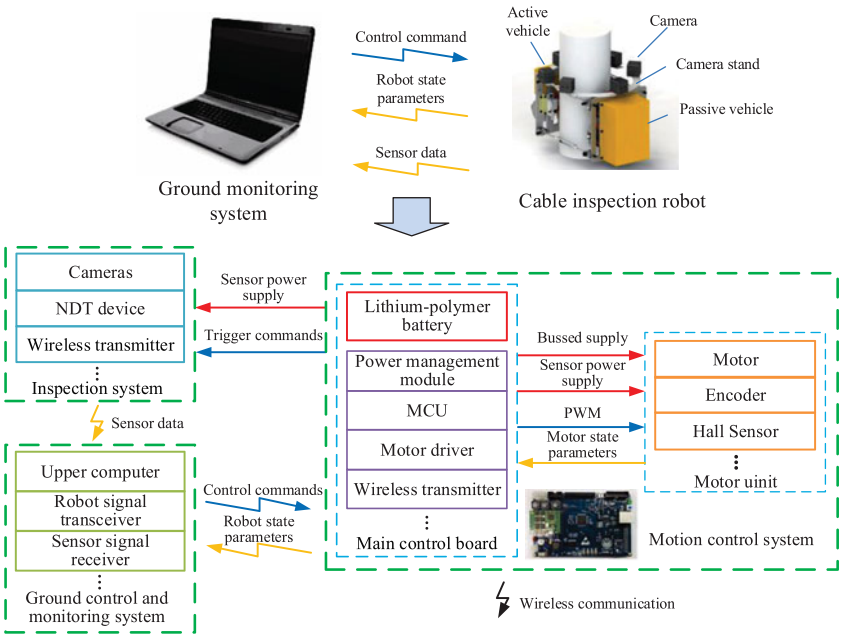

Fig. 8. Control system layout of the cable inspection robot.

3. Control System

The overall system of the cable inspection robot is illustrated in Fig. 8. The robot is deployed with six cameras capable of providing 360° real-time image and NDT devices (installed in free space of the passive vehicle). The control system is composed of a motion control system, an inspection system, and a ground control and monitoring system. The motion control system includes a main control board with a wireless transmitter and a motor. During the climbing process, the robot is controlled by the workstation remotely. In the meantime, the robot's state parameters such as the motor speed, driving current and battery level are transmitted to the ground workstation via the onboard wireless communication module. The inspection system includes sensors such as cameras, and the NDT devices. The sensor signals are converted and transmitted to the ground control and monitoring system through a high-bandwidth wireless transmitter. The inspection system is not discussed in detail in this paper. The ground control and monitoring system is consisted of a computer, a robot signal transceiver and a sensor signal receiver. Through the transceiver, the inspector can send out control commands and monitor running status of the robot.

https://doi.org/10.1017/S0263574720001253 Published online by Cambridge University Press

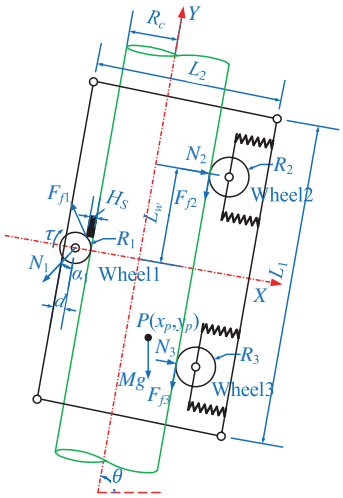

Fig. 9. Force model of active wheel obstacle crossing.

4. Analysis of the Obstacle Climbing Ability of the Robot

4.1. Force analysis of the robot

Figure 9 shows the force diagram of the robot in the case of active wheel climbing over obstacle. For simplifying the force analysis without over-reducing the calculation accuracy, it is appropriate to make assumptions as follows:

1. The robot climbs at a constant velocity.
2. The wheels of the robot do not slip during climbing.
3. The active wheel is only subject to the force applied by an obstacle at the instance of contact with an obstacle.
4. The compressed length of the four springs is the same.
5. The force applied to the passive wheels is not changed before and after the contact between the active wheel and the obstacle.

Based on assumptions (1)–(5), we can find a system of equations to describe the forces on the robot in the XY plane, which can be represented as:

$$\begin{aligned}
&\sum F_X = N_1 \sin\alpha_1 + F_{f1}\cos\alpha_1 - N_2 - N_3 - Mg\cos\theta = 0\\
&\sum F_Y = F_{f1}\sin\alpha_1 - N_1\cos\alpha_1 - F_{f2} - F_{f3} - Mg\sin\theta = 0\\
&\sum M_o = \tau + L_w(N_2 - N_3) + F_{f2}\left[R_1 + R_c\left(\sin\frac{\beta_1}{2} + \sin\frac{\beta_2}{2}\right)\right]\\
&\qquad + F_{f3}\left[R_1 + R_c\left(\sin\frac{\beta_1}{2} + \sin\frac{\beta_3}{2}\right)\right] + Mg\sin\theta\\
&\qquad \left(x_p + R_c\sin\frac{\beta_1}{2} + R_1\right) + Mg\cos\theta y_p - F_{f1}R_1 = 0
\end{aligned} \tag{5}$$

where M is the total mass of the robot, g is the gravity acceleration, R_1 is the equivalent radius of the active wheel, R_c is the radius of the cable, τ is the driving torque of the active wheel, β_i (i=1, 2, 3) is the angle of V groove of each wheel, θ is the tilt angle of the cable, x_p and y_p are the abscissa value and ordinate value of barycenter of the robot, respectively, L_w is the distance from the center of the passive wheel to the X axis, N_i (i=1, 2, 3) is the equivalent normal force applied to the wheels by the cable surface, F_{f1} is the friction driving force of the active wheel, F_{f2} and F_{f3} are friction

https://doi.org/10.1017/S0263574720001253 Published online by Cambridge University Press

Table II. Specifications of the robot.

Parameter	Value	Parameter	Value	Parameter	Value
μ_2	0.05	μ_3	0.05	τ_{max}	16.67 Nm
L_1	210 mm	L_2	250 mm	d	20 mm
L_w	60 mm	β_1	140°	β_2	150°
β_3	150°	R_1	26.75 mm	R_2	37.29 mm
R_3	37.29 mm	k	4.9 N/mm		

resistances of upper and lower passive wheels, respectively, and α_1 is the angle between the reacting normal force N_1 and cable axis, which can be represented as:

$$\sin\alpha_1 = 1 - \frac{H_s}{R_1}, \tag{6}$$

where H_s is the height of the obstacle.

F_{f2} and F_{f3} can be represented as:

$$F_{f2} = \frac{N_2\mu_2}{\sin(\beta_2/2)} \text{ and } F_{f3} = \frac{N_3\mu_3}{\sin(\beta_3/2)}, \tag{7}$$

where μ_2 and μ_3 are dynamic coefficients of the upper wheel and lower wheel, respectively.

According to assumptions (4) and (5), N_2 and N_3 are not changed before and after the active wheel contacts with the obstacle. Thus, we can get:[19]

$$N_2 + N_3 = 4k\Delta x - M_s g\cos\theta, \tag{8}$$

where k is the stiffness of each spring, M_s is the mass of the passive vehicle and Δx is the compressed length of the spring, which can be given by:

$$\Delta x = X_0 - \left[L_2 - d - R_1 - R_2 - R_c\left(\sin\frac{\beta_1}{2} + \sin\frac{\beta_2}{2}\right)\right], \tag{9}$$

where X_0 is the initial distance of the spring, L_2 is the length of the turnbuckle, d is the mounting distance of the active wheel and R_2 is the equivalent radius of the upper passive wheel, which is equal to that of the lower passive wheel.

According to moment balance, we can get:

$$\tau = F_{f1}R_1. \tag{10}$$

Based on Eqs. (5)–(10), N_1, N_2, N_3, F_{f1} and τ can be calculated. Thus, the force state of the robot during climbing obstacle can be obtained. The constraint conditions for robot obstacle crossing are as follows:

$$\mu_1 N_1\sin\alpha_1 \geq (N_1\cos\alpha_1 + F_{f2} + F_{f3} + Mg\sin\theta)\sin\frac{\beta_1}{2}, \tag{11}$$

$$\tau_{max} \geq \frac{(N_1\cos\alpha_1 + F_{f2} + F_{f3} + Mg\sin\theta)R_1}{\sin\alpha_1}, \tag{12}$$

where τ_{max} is the maximum driving torque of the motor, and μ_1 is the static friction coefficient. Equations (11) and (12) are the slipless condition and driving condition for the active wheel in the case of obstacle crossing, respectively. The total resistance of the robot can be represented as:

$$F_r = N_1\cos\alpha_1 + F_{f2} + F_{f3} + Mg\sin\theta. \tag{13}$$

According to the force model, the driving force, resistance and obstacle height can be calculated. The main parameters of the climbing robot and the cable are listed in Table II.

The analytical methods of the upper passive wheel and lower passive wheel for climbing obstacle are identical to that of the active wheel, and we can obtain climbing capability according to the static force model. Figure 10a–(c) depicts the results of the active wheel, upper passive wheel and lower

https://doi.org/10.1017/S0263574720001253 Published online by Cambridge University Press

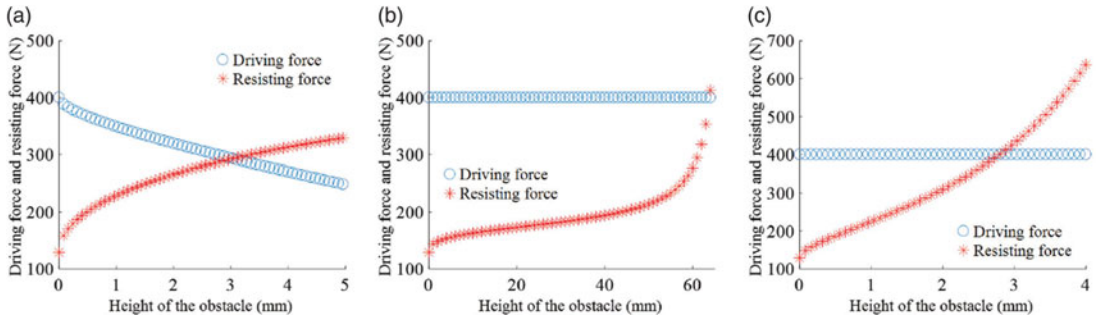

Fig. 10. The relationships of the driving force and resistance with obstacle height. (a) Active wheel climbing obstacle. (b) Upper passive wheel climbing obstacle. (c) Lower passive wheel climbing obstacle.

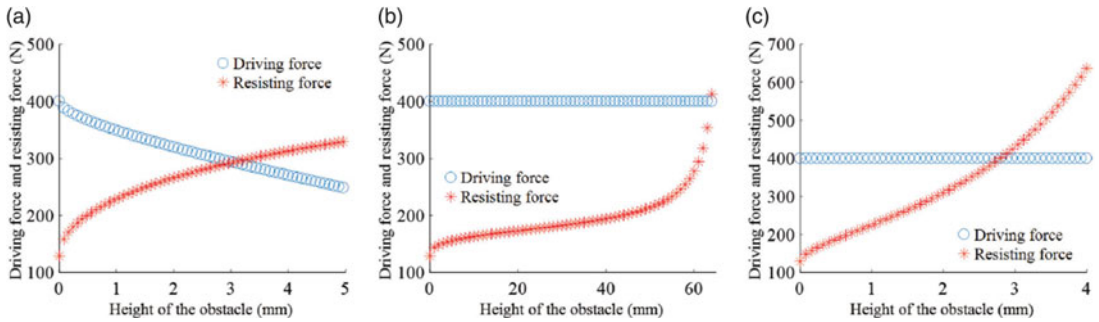

Fig. 11. The obstacle climbing ability of the robot with different cable radii and preload forces. (a) Active wheel. (b) Lower passive wheel.

passive wheel, respectively. The tilt angle of the cable is 70°. The blue curve represents the maximum driving force. The red curve represents the total resisting force. The intersection point of these two curves indicates the maximum height of the surmounting obstacle for the climbing robot. The results show that the upper passive wheel has stronger obstacle-negotiation capability than the active wheel and lower passive wheel. This is because the barycenter of the robot is close to the lower passive wheel.

4.2. The effect of cable radius on obstacle climbing ability

The robot climbing ability with different cable radii is analyzed based on the force model mentioned above. The range of cable radius and spring compressed length are 45–100 mm and 20–30 mm, respectively. The tilt angle of the cable is 70°. Other parameters are the same with Table II.

The maximum height of surmounting obstacle of the climbing robot with different cable radii and preload forces is shown in Fig. 11. The results indicate that under a fixed cable radius condition, the obstacle climbing ability of the active wheel improves with the increase of preload force. The variation in climbing ability with cable radius also has the same trend, as shown in Fig. 11(a). In the case of passive wheel climbing obstacle (take lower passive wheel for example), the maximum height of surmounting obstacle improves with the increase of preload force, as shown in Fig. 11(b). This is similar to the active wheel. However, the climbing ability decreases with increased cable radius. It is important to note that the obstacle performance of the robot may be declined with the increase of preload force because too large preload force increases friction resistance. Therefore, it is necessary to select proper preload force range for the installation and operation of the cable inspection robot. The climbing capability of the upper passive wheel can be obtained by the identical method.

4.3. The effect of cable tilt angle on obstacle climbing ability

The robot climbing ability with different cable tilt angles and preload forces is analyzed based on the force model mentioned above. The variation range of cable tilt angles is 30–90°. The radius of the cable is 55 mm. Other parameters are the same with Table II.

https://doi.org/10.1017/S0263574720001253 Published online by Cambridge University Press

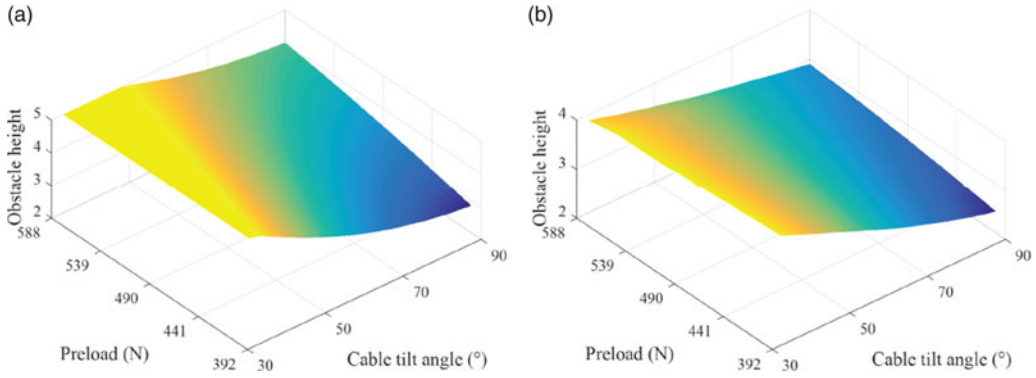

Fig. 12. The obstacle climbing ability of the robot with different cable tilt angles and preload forces. (a) Active wheel. (b) Lower passive wheel.

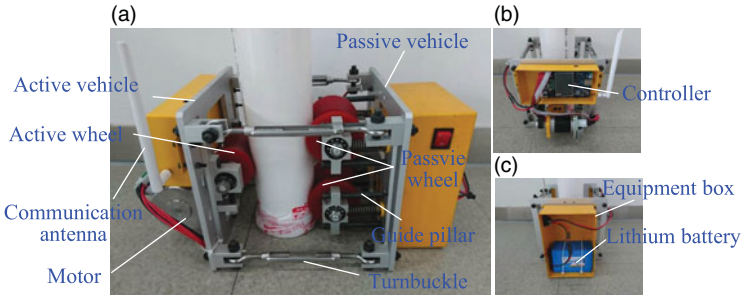

Fig. 13. Laboratory experiment. (a) Prototype of the robot. (b) Front view of active vehicle. (c) Front view of passive vehicle.

The maximum heights of surmounting obstacle of the climbing robot with different cable tilt angles and preload forces are illustrated in Fig. 12. The results indicate that under a fixed tilt angle condition, the obstacle climbing ability of the active wheel improves with the increase of preload force. However, the variation in climbing ability with tilt angle has an opposite trend, as shown in Fig. 12(a). It is noticed that the height of surmounting obstacle reaches the maximum values at the tilt range of 30–50°. This is because the driving torque of the motor reaches the maximum value. In the case of lower passive wheel climbing obstacle, the obstacle climbing ability improves with the increase of preload force and decreases with the increase of the cable tilt angle, as shown in Fig. 12(b). This is similar to the active wheel. The analytical method of the upper passive wheel is also identical to that of the active wheel and lower passive wheel.

5. Experiments

In order to verify the effectiveness of the robot, its climbing performance was tested in the lab. The experimental environment is configured with a 110 mm diameter polyvinyl chloride (PVC) pipe of 2 m long, as shown in Fig. 13(a). As mentioned above, the robot is consisted of an active vehicle and a passive vehicle connected by four turnbuckles, which can be completely installed within 2 min by two workers. Figure 13(b) and (c) shows the front views of active vehicle and passive vehicle, respectively. The main control board of the robot is installed in the equipment box of the active vehicle. The lithium-polymer battery is installed in the equipment box of the passive vehicle. In addition, the free space in the equipment box of the passive vehicle can be used to install additional NDT devices.

5.1. Climbing capability experiment

Figure 14 shows the driving torque curve of the BLDC motor with different cable tilt angles. The experiments are carried out with the same climbing speed. The red curve represents the experimental value of the driving torque. The blue curve represents the theory value of the driving torque based on the force model mentioned in Section 4. The results indicate that this robot can steadily climb without

https://doi.org/10.1017/S0263574720001253 Published online by Cambridge University Press

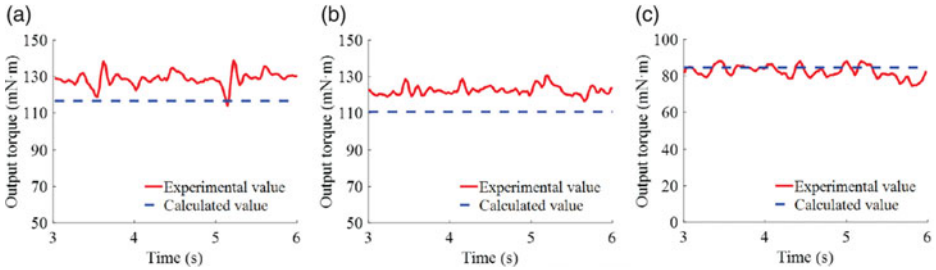

Fig. 14. The effect of cable tilt angle on BDLC motor driving torque. (a) 90° cable. (b) 70° cable. (c) 40° cable.

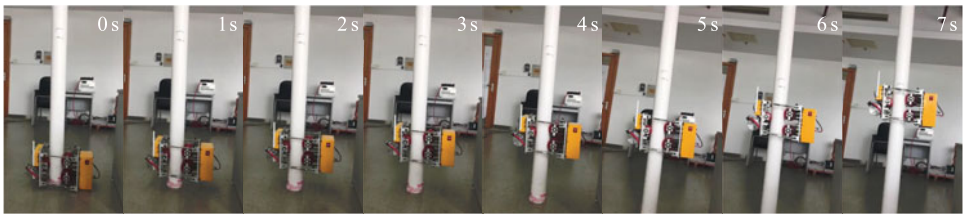

Fig. 15. Robot climbing capacity experiment.

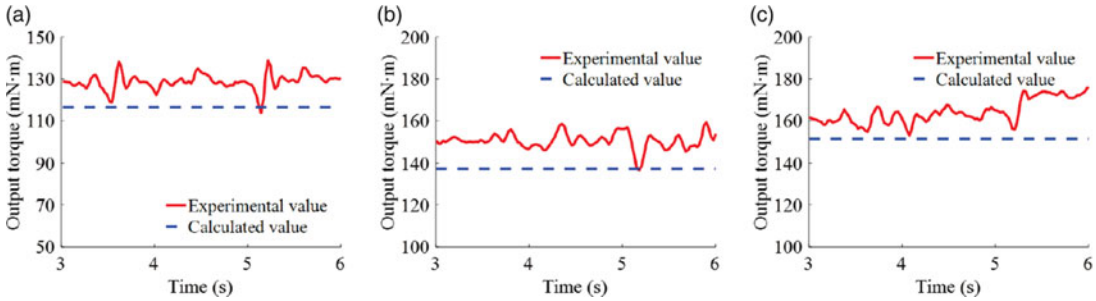

Fig. 16. The effect of payload on BDLC motor driving torque. (a) no-load. (b) 3 kg. (c) 5 kg.

deflection. The experimental values show consistencies with the theoretical values. There are some errors between the experimental curve and theoretical values. These errors are mainly caused by the non-coincidence between the theory mass center and actual center of the robot, machining error and other uncontrolled factors. The results also show that the driving torque improves with the increase of the cable tilt angle. Figure 15 shows the photo snapshots when the robot climbs up a vertical cable. During the climbing process, the active wheel does not slip, indicating that the static friction coefficient satisfies with the climbing requirements.

Figure 16 shows the driving torque curve of the BLDC motor with different payloads on a vertical cable. The experiments are carried out with the same climbing speed. The red and blue curves represent the experimental value and theory value of the driving torque, respectively. The results show that the driving torque improves with the increase of payload. The experimental results also show consistencies with the theoretical values. This demonstrates the effectiveness of the proposed model.

5.2. Obstacle climbing ability of active vehicle

To verify the ability of the active vehicle to overcome obstacles, gaskets and nuts are used as obstacles for the climbing robot, as shown in Fig. 17. The thickness of the gasket and nut is 1.5 and 2.42 mm, respectively.

Take the obstacle of 2.42 mm height for example, the ability to overcome obstacle of the active vehicle with different payloads is verified by experiments. The experiments were carried out with the same climbing speed and the tilt angle of the cable is 90°. Figure 18(a) shows that the motor speed drops firstly at the beginning of contact with the obstacle, and then increases. The impact causes the loss of motor speed. Thus, the Proportion Integration Differentiation (PID) controller increases the

https://doi.org/10.1017/S0263574720001253 Published online by Cambridge University Press

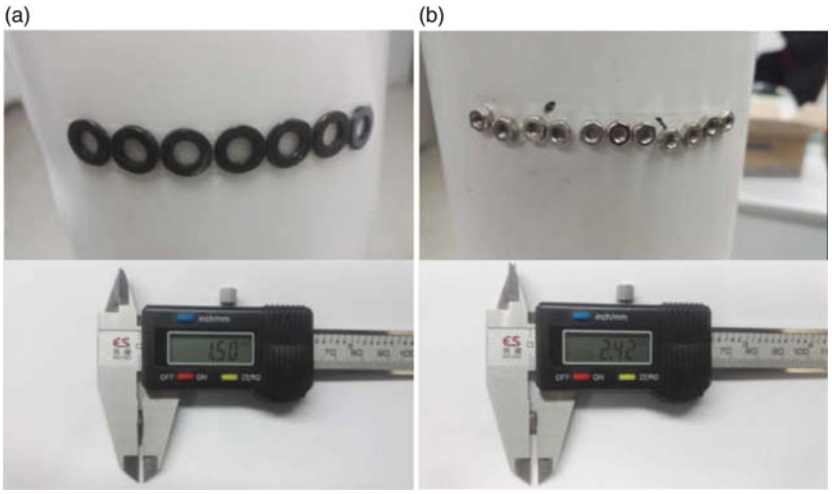

Fig. 17. Robot climbing capacity experiment. (a) 1.5 mm height obstacle. (b) 2.42 mm height obstacle.

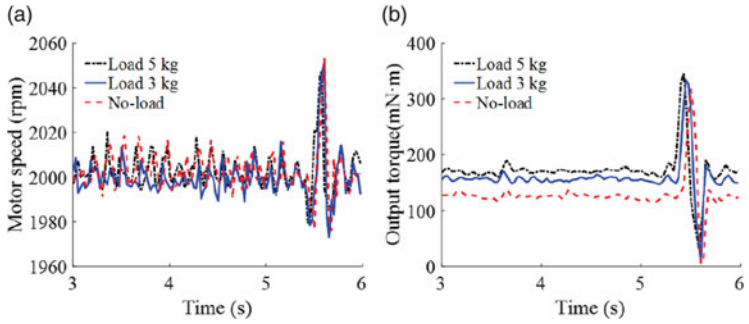

Fig. 18. Active vehicle obstacle climbing experiment (2.42 mm height obstacle). (a) The speed of motor. (b) The driving torque of motor.

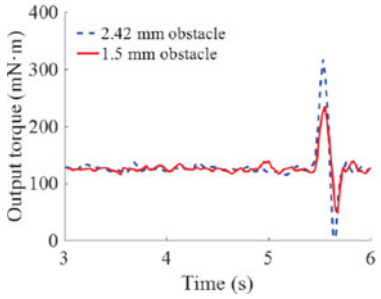

Fig. 19. Driving torque with different heights of obstacle in the case of active vehicle obstacle climbing (90°).

duty cycle of the drive circuit. This leads to the overshoot of the motor speed. The results in Fig. 18(a) also indicate that the speed fluctuation decreases with the increase of the payload. The driving torque curve during the process of obstacle climbing is shown in Fig. 18(b). The figure indicates that the driving torque increases rapidly to offset the obstacle resistance at the beginning of contact with the obstacle. Before and after overcome the obstacle successfully, the driving torque keeps stable, which is consistent with Fig. 16. The results also indicate that the driving torque improves with the payload increases.

Figure 19 shows the non-load driving torque with different heights of obstacle in the case of active vehicle obstacle climbing. The results indicate that the driving torque under the two conditions is almost the same before obstacle climbing. During the process of obstacle climbing, the fluctuation of driving torque with 2.42 mm height obstacle is greater than that with 1.5 mm height obstacle. Figure 20 shows the photo snapshots of the active vehicle obstacle climbing experiment.

https://doi.org/10.1017/S0263574720001253 Published online by Cambridge University Press

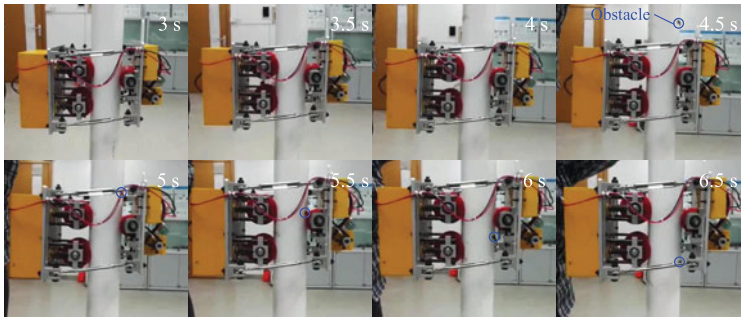

Fig. 20. Active vehicle obstacle climbing experiment (1.5 mm height obstacle).

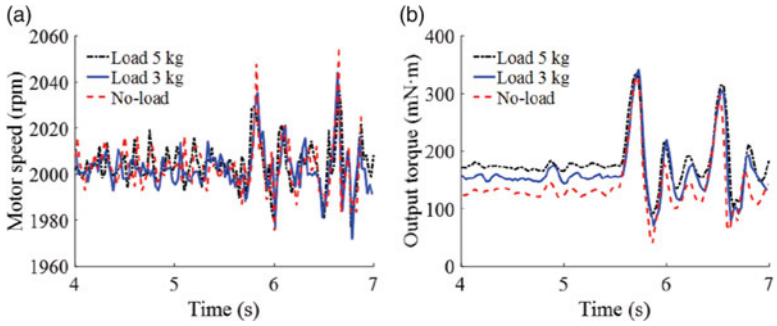

Fig. 21. Passive vehicle obstacle climbing experiment (2.42 mm height obstacle). (a) The speed of motor. (b) The driving torque of motor.

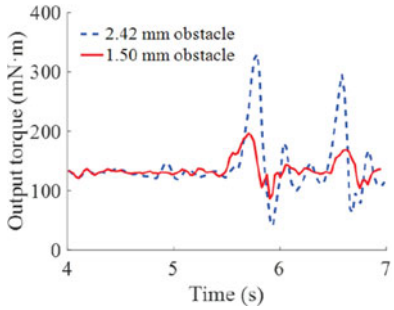

Fig. 22. Driving torque with different heights of surmounting obstacle in the case of passive vehicle obstacle climbing (90°).

5.3. Obstacle climbing ability of passive vehicle

Take the obstacle of 2.42 mm height for example, the ability to overcome obstacle of the passive vehicle with different payloads is verified by experiments, as shown in Fig. 21. The experiments are carried out with the same climbing speed and the tilt angle of the cable is 90°. The variation trends of the motor speed and driving torque are similar to the active vehicle obstacle climbing. It should be noted that the experimental results have two peaks because the passive vehicle has two passive wheels to climb over obstacles. This is different from the active vehicle obstacle climbing.

Figure 22 shows the non-load driving torque with different heights of obstacle in the case of passive vehicle obstacle climbing. The results are similar to that of active vehicle obstacle climbing. The driving torques of the two conditions are approximately the same on the smooth cable surface. In the case of obstacle climbing, the driving torque with a higher obstacle is larger than that with lower obstacle. Figure 23 shows the photo snapshots of the passive vehicle obstacle climbing experiment.

5.4. Safe landing experiment

In order to verify the ability of safe landing of the robot, the power was shut off when the robot reached the top of the PVC pipe, as shown in Fig. 24. The total mass of the robot including the

https://doi.org/10.1017/S0263574720001253 Published online by Cambridge University Press

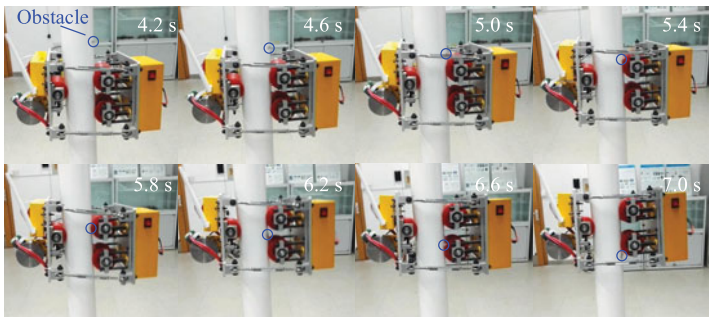

Fig. 23. Passive vehicle obstacle climbing experiment (with obstacle height of 2.4 mm).

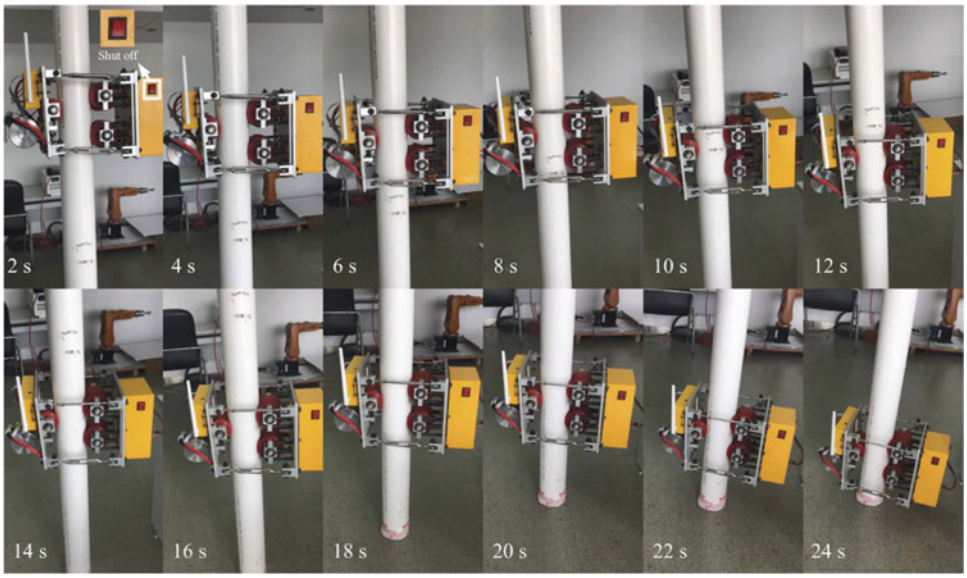

Fig. 24. Safe landing experiment.

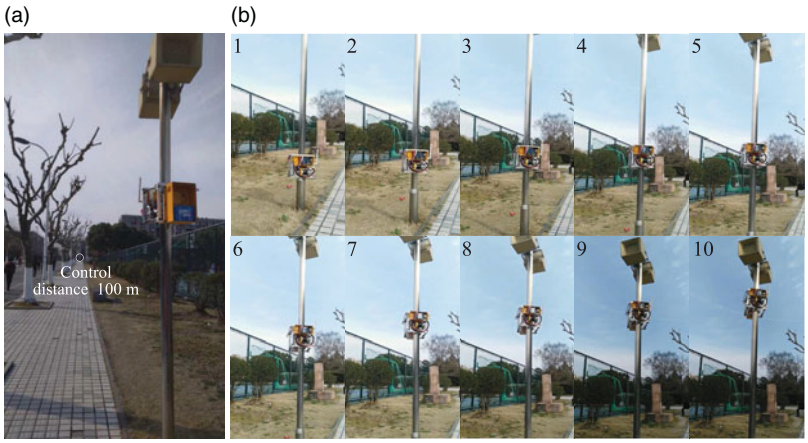

Fig. 25. Outdoor environmental experiment. (a) Robot climb with a vertical pole 90 mm in diameter. (b) Climbing test.

lithium battery is 12 kg. The one-way damper was operated automatically after the power loss. The results show that the robot descended safely at approximately a speed of 60 mm/s. The speed can be modulated by tuning the damper. However, in the case of getting stuck on the cable, the robot can be pulled back to the ground by a rescue climbing robot with electromagnetic or mechanical adsorption device.

https://doi.org/10.1017/S0263574720001253 Published online by Cambridge University Press

5.5. Outdoor environmental experiment

Outdoor environmental experiment is conducted with a vertical pole of 90 mm in diameter, as shown in Fig. 25(a). The total mass of the robot including the lithium battery is 12 kg. The remote distance is about 100 m. The robot stably climbed up approximately 3 m of the pole at a speed of 9 m/min, as shown in Fig. 25(b). The experiment verifies the reliability of long-distance communication of the wireless robot control system. Furthermore, the adaptability to different pipe diameter and surface of the robot is also proved.

6. Conclusion

In this paper, a new lightweight cable inspection robot based on wireless control is proposed. The cable-climbing robot is a wireless mobile platform with inspection and maintenance equipment. The novel mechanisms for the robot are proposed under the environmental conditions of cable-stayed bridges. The robot is composed of two vehicles connected by four turnbuckles. Its driving mechanism adopts a V type wheel driven by a BLDC motor, and the turnbuckles ensure simple and quick installation procedure. Compared to most of the existing cable inspection robots, the preload force (normal force) of the preload mechanism during the installation procedure can be adjusted continuously and measured by the scale on the guide pillar. The one-way rotating damper for electrical malfunction or power failure situations guarantees the safety retrieval of the robot. The static force model of the robot during obstacle climbing is developed. The relationships of the driving force and resistance with different obstacle heights to determine the obstacle climbing ability of the robot are obtained. The effects of the cable diameter, cable inclination and preload force on obstacle climbing ability of the robot are also analyzed. The experiments verify that the robot could climb random inclined cables and overcome an obstacle of 2.42 mm in height with a mass of 5 kg payload. This research provides the theoretical and practical references for the development of the automatic cable or pole-like structure inspection mechanism.

For the future works, the field test will be carried out to study factors that influence the energy consumption of the robot. The rescue method will be also studied to avoid the robot getting stuck on the cable at high altitude. In addition, we plan to study the wireless control strategy and images inspection method.

Acknowledgements

The work was supported by National Key R&D Program of China (Grant No. 2018YFB1306903), National Natural Science Foundation of China (Grant No. 51975415, U1713215 and 51705368), the Fundamental Research Funds for the Central Universities (Grant No. 22120180562), Major Project of Special Development Fund for Shanghai Zhangjiang National Independent Innovation Demonstration Zone (Grant No. ZJ2019-ZD-003).

References

1. H. M. La, T. H. Dinh, N. H. Pham, Q. P. Ha and A. Q. Pham, "Automated robotic monitoring and inspection of steel structures and bridges," *Robotica* (2018). doi:10.1017/S0263574717000601
2. A. B. Mehrabi, C. A. Ligozio, A. T. Ciolko and S. T. Wyatt, "Evaluation, rehabilitation planning, and stay-cable replacement design for the Hale Boggs Bridge in Luling, Louisiana," *J. Bridge Eng.* **15**(4), 364–372 (2010).
3. D. Pagano and D. Liu, "An approach for real-time motion planning of an inchworm robot in complex steel bridge environments," *Robotica* **35**(6), 1280–1309 (2017).
4. Y. Tian and F. Gao, "Efficient motion generation for a six-legged robot walking on irregular terrain via integrated foothold selection and optimization-based whole-body planning," *Robotica* **36**(3), 333–352 (2018).
5. B. He, Z. Wang, M. Li, K. Wang, R. Shen and S. Hu, "Wet adhesion inspired bionic climbing robot," *IEEE/ASME Trans. Mechatron.* **19**(1), 312–320 (2014).
6. J. Luo, S. Xie, Z. Gong and T. Lu, "Development of cable maintenance robot for cable-stayed bridges," *Ind. Robot* **34**(4), 303–309 (2007).
7. Y. Guan, L. Jiang, H. Zhu, X. Zhou, C. Cai, W. Wu, Z. Li, H. Zhang and X. Zhang, "Climbot: A Modular Bio-Inspired Biped Climbing Robot," *Proceedings of the IEEE/RSJ International Conference on Intell. Robots Syst.* (2011) pp. 1473–1478.
8. Y. Guan, L. Jiang, H. Zhu, W. Wu, X. Zhou, H. Zhang and X. Zhang, "Climbot: A bio-inspired modular biped climbing robot system development, climbing gaits, and experiments," *J. Mech. Robot.* **8**(2), 021026 (2016).

9. T. L. Lam and Y.Xu, "A Flexible Tree Climbing Robot: Treebot-Design and Implementation," *International Conference on Robotics and Automation* (2011) pp. 5849–5854.
10. T. L. Lam and Y. Xu, "Biologically inspired tree-climbing robot with continuum maneuvering mechanism," *J. Field Robot.* **29**(6), 843–860 (2012).
11. S. Mahdavi, E. Noohi and M. N. Ahmadabadi, "Basic Movements of a Nonholonomic Wheel-Based Pole Climbing Robot," *International Conference on Advanced Intelligent Mechatronics* (2007) pp. 1–6.
12. M. Tavakoli, M. R. Zakerzadeh, G. Vossoughi and S. Bagheri, "A hybrid pole climbing and manipulating robot with minimum DoFs for construction and service applications," *Ind. Robot* **32**(2), 171–178 (2005).
13. A. Mazumdar and H. H. Asada, "Mag-foot: A Steel Bridge Inspection Robot," *Proceedings of the IEEE/RSJ International Conference on Intelligent Robots and Systems* (2009) pp. 1691–1696.
14. E. Kuhn, "Maintenance with Industrial Rope Access: Uddevalla Bridge-a Case Study," *IABSE Symposium Report*, vol. 91(1) (2006) pp. 1–3.
15. J. J. Lee, J. M. Kim, S. S. Ahn and J. S. Choi, "Development of a cable exciter to evaluate damping ratios of a stay cable," *KSCE J. Civ. Eng.* **14**(3), 363–370 (2010).
16. H. N. Ho, K. D. Kim, Y. S. Park and J. J. Lee, "An efficient image-based damage detection for cable surface in cable-stayed bridges," *Ndt E Int.* **58**(9), 18–23 (2013).
17. K. H. Cho, Y. H. Jin, H. M. Kim, H. Moon, J. C. Koo and H. R. Choi, "Caterpillar-Based Cable Climbing Robot for Inspection of Suspension Bridge Hanger Rope," *Proceedings of the IEEE International Conference on Automation Science and Engineering* (2013) pp. 1059–1062.
18. K. H. Cho, H. M. Kim, Y. H. Jin, F. Liu, H. Moon, J. C. Koo and H. R. Choi, "Inspection robot for hanger cable of suspension bridge: Mechanism design and analysis," *IEEE/ASME Trans. Mechatron.* **18**(6), 1665–1674 (2013).
19. K. H. Cho, Y. H. Jin, H. M. Kim, H. Moon, J. C. Koo and H. R. Choi, "Multifunctional robotic crawler for inspection of suspension bridge hanger cables: Mechanism design and performance validation," *IEEE/ASME Trans. Mechatron.* **22**(1), 236–246 (2017).
20. H. P. Huang, J. L. Yan and T. H. Cheng, "Development and fuzzy control of a pipe inspection robot," *IEEE Trans. Ind. Electron.* **57**(3), 1088–1095 (2010).

https://doi.org/10.1017/S0263574720001253 Published online by Cambridge University Press